Journal of Materials Chemistry A

RSC Publishing

PAPER

View Article Online
View Journal | View Issue

Unveiling organic–inorganic hybrids as a cathode material for high performance lithium-ion capacitors†

Cite this: *J. Mater. Chem. A*, 2013, **1**, 707

K. Karthikeyan,[a] S. Amaresh,[a] V. Aravindan,[ab] H. Kim,[c] K. S. Kang[c] and Y. S. Lee*[a]

Received 4th October 2012
Accepted 12th October 2012

DOI: 10.1039/c2ta00553k

www.rsc.org/MaterialsA

Novel Li-ion hybrid supercapacitors were developed containing composite cathodes of a conducting polymer – either polyaniline (PANI) or polypyrrole (PPy) – with $Li(Mn_{1/3}Ni_{1/3}Fe_{1/3})O_2$ nanoparticles. Activated carbon (AC) anodes were used in the presence of an organic electrolyte. Using a PANI composite electrode resulted in a cell with outstanding supercapacitive behavior, even at high currents. It showed better cycleability than the cells using a PPy composite electrode or pristine material. The cell with a PANI composite electrode delivered high specific capacitances of 140, 93, and 56 F g^{-1} at current densities of 0.72, 1.45 and 2.15 A g^{-1}, respectively. The observed capacitances are the best yet reported for hybrid supercapacitors based on Li-intercalating materials in organic electrolytes. The hybrid supercapacitor containing PANI delivered maximum energy and power densities of 49 W h kg^{-1} and 3 kW kg^{-1}, respectively. These results demonstrate the potential of developing polymer-encapsulated, Li-intercalating materials for high-performance, Li-ion, hybrid supercapacitors.

Introduction

In efforts to reduce CO_2 emissions, much work has sought to develop more efficient and more reliable energy storage devices for use in zero-emission transportation, particularly electric vehicles and hybrid electric vehicles. Hybrid supercapacitors (HSCs) are electrochemical energy storage devices that combine the advantages of both Li-ion cells and supercapacitors.[1,2] They are expected to bridge the gap between Li-ion cells and supercapacitors and be used to power electric and hybrid vehicles.[3] They can deliver high energy and power densities for short periods with long cycle lives, while operating over a wide range of temperatures with low maintenance costs.[4–6]

Generally, an HSC is a single device containing a Li-insertion type electrode (battery component) and an electric double layer forming component (supercapacitor element) as a counter electrode in either aqueous or non-aqueous medium.[2] Such Li-ion hybrid supercapacitors (Li-HSCs) can deliver higher energy density than supercapacitors and higher power density than Li-ion batteries. They are also stable over long-term cycling. Carbon-based materials are generally considered best for the supercapacitive component because of their high specific surface area, good electronic conductivity, cycleability, low cost and low environmental impact. Carbonaceous materials also exhibit high stability and strong cycling lives in any electrolyte.[7–10] Although several inorganic binary oxides, such as Co_3O_4, NiO, TiO_2, and MnO_2, have been tested for use in supercapacitors in aqueous media,[11–15] water splitting (at ~1.23 V) restricts their use in high-energy applications, such as vehicles. Therefore, research has focused largely on the development of non-aqueous Li-HSCs.

Such non-aqueous devices were first reported by Amatucci *et al.*[1,2] using various Li-insertion materials with activated carbon (AC). Several Li-intercalating materials have since been reported for Li-HSC applications.[14,16–27] Among them, Mn-based intercalating materials are promising for use in Li-HSC applications due to their low environmental impact, natural abundance and low cost.[28] However, Mn based materials, for example $LiMn_2O_4$, experience capacity fading during cycling either in native or doped forms ($LiM_xMn_{2-x}O_4$, M = Ni, Cr, Al, and Co).[29,30] The polyanion framework Li_2MSiO_4 (M = Mn and Fe) has been tested as a low-cost electrode material for Li-HSCs with AC counter electrodes,[31,32] although its performance is not sufficient to power electric or hybrid electric vehicles. The search continues for suitable, high-performance, Li-insertion electrodes.

As part of such efforts, this work reports the preparation and characterization of inherent layered type $Li(Mn_{1/3}Ni_{1/3}Fe_{1/3})O_2$ cathodes as low-cost, high-capacity Li-insertion type materials for Li-HSCs with low environmental impact. The parent $Li(Mn_{1/3}Ni_{1/3}Co_{1/3})O_2$ is used as a high-performance and high-capacity cathode in Li-ion batteries. Here, its toxic Co was replaced by Fe.[33] Replacement of Co by Fe in the layered matrix reduces the electronic conducting profile and the use of the

[a]*Faculty of Applied Chemical Engineering, Chonnam National University, Gwangju 500-757, Korea. E-mail: leeys@chonnam.ac.kr*

[b]*Energy Research Institute @ NTU (ERI@N), Research techno Plaza, Nanyang Technological University, Singapore 637553. E-mail: aravind_van@yahoo.com*

[c]*Department of Materials Science and Engineering, Seoul National University, Seoul 151-742, Korea*

† Electronic supplementary information (ESI) available. See DOI: 10.1039/c2ta00553k

$Fe^{3+/4+}$ couple is very difficult.[34] Therefore, conduction coatings or composites are necessary to achieve high-performance, Li-insertion electrodes.

Organic and inorganic composites are potentially useful electrodes for supercapacitors.[35–39] Composites of transition metal oxides (TMOs) with conducting polymers like polyaniline (PANI), polypyrrole (PPy), and poly(3,4-ethylenedioxythiophene) (PEDOT) have been explored. Composite hybrids tested as Li-insertion electrodes in Li-ion cells include $LiFePO_4$, $LiNi_{0.8}Co_{0.2}O_2$ and $Li(Mn_{1/3}Ni_{1/3}Co_{1/3})O_2$ with conducting polymers.[40–44] However, to the best of our knowledge the electrochemical performances of such hybrids as active materials in non-aqueous Li-HSCs have yet to be reported.

Hence, this work explores the use of organic–inorganic composites as Li-insertion electrodes with either PANI or PPy in Li-HSCs. Unlike carbon coating, conducting polymers are physically bound to the TMO and thereby increase the overall surface area, providing more active sites for electrochemical reactions. The polymer network also enhances Li-ion movement to maximize electrolyte access. Here, the electrochemical supercapacitive performances of pristine $Li(Mn_{1/3}Ni_{1/3}Fe_{1/3})O_2$ and chemically prepared $Li(Mn_{1/3}Ni_{1/3}Fe_{1/3})O_2$–PANI and $Li(Mn_{1/3}Ni_{1/3}Fe_{1/3})O_2$–PPy composites were assessed in two-electrode asymmetric configurations with AC electrodes in the presence of 1 M $LiPF_6$ (1 : 1 EC : DMC; v/v) electrolyte.

Experimental section

Synthesis of $Li(Mn_{1/3}Ni_{1/3}Fe_{1/3})O_2$

A mixed hydroxide route was used to prepare $Li(Mn_{1/3}Ni_{1/3}Fe_{1/3})O_2$ nanoparticles. In a typical synthesis, stoichiometric amounts of $Fe(NO_3)_3 \cdot 9H_2O$ (Junsei chemicals, Japan 98%), $MnCl_2 \cdot 4H_2O$ (Wako, Japan 99.9%) and $Ni(NO_3)_3 \cdot 6H_2O$ (Junsei chemicals, Japan 97%) were dissolved separately in distilled water and then mixed together. Aqueous LiOH (Junsei chemicals, Japan 95%) was then added drop wise to the mixture to yield hydroxide precipitate, which was aged overnight, filtered and washed to remove residual Li moieties and vacuum dried at 60 °C for 10 h in air. $Li(Mn_{1/3}Ni_{1/3}Fe_{1/3})O_2$ was obtained by sintering the precipitates with a slight excess of LiOH at 800 °C for 10 h under an oxygen flow.

Preparation of composite hybrids

Composites were prepared by chemical polymerization. In a typical procedure, an appropriate amount of $Li(Mn_{1/3}Ni_{1/3}Fe_{1/3})O_2$ (0.1 g) was added to 0.2 mmol aqueous monomer. Oxidant was then added to this mixture at a monomer to oxidant ratio of 1 : 1. The $Li(Mn_{1/3}Ni_{1/3}Fe_{1/3})O_2$–PANI hybrid composite was synthesized through oxidative polymerization of aniline by ammonium persulphate (APS) in 50 ml 1 M HCl (Fig. 1). Here, APS acts as an oxidant that initiates the monomer for the polymerization process in which HCl acts as a dopant to enhance the conductivity of the polymer matrix. The polymerization process occurred during the sonication of $Li(Mn_{1/3}Ni_{1/3}Fe_{1/3})O_2$ particles along with a PANI monomer for the preparation of composite hybrids. The schematic representation of the synthesis process of a composite hybrid is clearly illustrated in Fig. 1. The PPy composite was prepared by adding pyrrole to 50 ml 1 M H_2SO_4 containing $Li(Mn_{1/3}Ni_{1/3}Fe_{1/3})O_2$ and $FeCl_3$. In this case, $FeCl_3$ acted as an oxidant and H_2SO_4 as a dopant. The experimental conditions – concentration of monomer and oxidant, time and temperature for preparing PANI and PPy composites – were unvaried throughout the syntheses. Only the monomers varied.

Characterization

The powders' phase purity was examined by X-ray diffractometry (XRD, Rint 1000, Regaku, Japan) using Cu Kα radiation. Samples' morphologies were observed by scanning electron microscopy (FE-SEM, S4700, Hitachi, Japan) and transmission electron microscopy (TEM, JEM-2000 FX-II, JEOL, Japan).

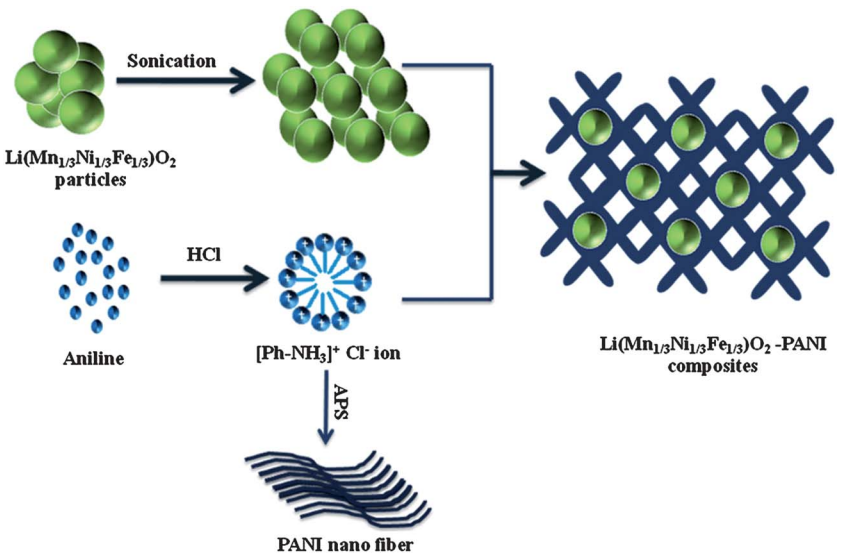

Fig. 1 The synthesis of the $Li(Mn_{1/3}Ni_{1/3}Fe_{1/3})O_2$–PANI composite hybrid through chemical polymerization.

Fourier transform infrared (FT-IR) spectroscopy was conducted on an IRPresitge-21 spectrometer, Japan. Brunauer–Emmett–Teller (BET) surface area analysis was performed using an ASAP 2010 surface analyzer (Micromeritics, USA).

Electrochemical studies

Electrodes for Li-HSCs were prepared by pressing on nickel mesh (area 200 mm^2) slurries of the electroactive materials mixed with a conducting additive (Ketjen black) and teflonized acetylene black binder at a weight ratio of 80 : 10 : 10. The pressed meshes were dried at 160 °C for 4 h in a vacuum. Test cells were fabricated in a CR 2032 coin cell configuration in an argon-filled glove box by sandwiching a cathode and an anode separated by a porous polypropylene separator (Celgard 3401). The cells were filled with an electrolyte of 1 M $LiPF_6$ in ethylene carbonate (EC)/dimethyl carbonate (DMC) (1 : 1 v/v). Electrochemical impedance spectroscopy (EIS) and cyclic voltammetry at different scan rates were performed using an electrochemical workstation (SP-150, Bio-Logic, France). Galvanostatic charge–discharge studies were conducted between 0 and 3 V using a cycle tester (WBCS3000, Won-A-Tech, Korea) at different current densities at ambient temperature. Electrochemical parameters such as specific capacitance (F g^{-1}), columbic efficiency (%), specific power density (W kg^{-1}) and energy density (W h kg^{-1}) were calculated according to established formulae.[16–19]

Results and discussion

The XRD pattern of $Li(Mn_{1/3}Ni_{1/3}Fe_{1/3})O_2$ powder prepared at 800 °C was refined by assuming a $R\bar{3}m$ space group with Li atoms in 3*a* sites, Mn, Ni and Fe atoms in 3*b* sites and O atoms in 6*c* sites (Fig. 2a). The observed XRD reflections fit well with the Bragg positions, which confirmed a characteristic layered material with the $R\bar{3}m$ space group. In the XRD reflections, the $I_{(003)}/I_{(104)}$ intensity ratio and clear splitting of the (006)/(102) and the (108)/(110) peaks are indicative of a typical layered material. The spectra show low cation disordering between the Li (3*a*) and the transition metal sites (3*b*) of the hexagonal layered structure.[33,44] Lattice parameters of $a = 2.898$ and $c = 14.311$ with a c/a ratio of 4.94 were observed, in good agreement with results for a similar layered compound, $Li(Mn_{1/3}Ni_{1/3}Co_{1/3})O_2$, reported by Yabuuchi and Ohzuku.[33]

The XRD patterns of native and polymer-encapsulated $Li(Mn_{1/3}Ni_{1/3}Fe_{1/3})O_2$ (Fig. 2b) are indexed based on a hexagonal α-$NaFeO_2$ structure with a $R\bar{3}m$ space group. They indicate the formation of a phase pure structure without any impurities or polymers – PPy or PANI. The absence of polymer peaks is due mainly to the very low concentrations of PANI and PPy being insufficient to be detected by an X-ray diffractometer. The similar spectra with no shifted peak positions indicate that in both composites the presence of organic moieties did not affect the structural properties of the layered matrices during polymerization.[46] Overall, all the samples showed well-developed layered structures.[33,44] To confirm the presence of the polymers, FT-IR spectra were recorded (Fig. 2c). $Li(Mn_{1/3}Ni_{1/3}Fe_{1/3})O_2$ did not show any peaks at >600 cm^{-1}, whereas the hybrid composites did, indicating the presence of organic moieties. The PPy composites show a peak at ~1560 cm^{-1} associated with the combination of C–C and C=C stretching vibrations of pyrrole rings.[47] The bands at ~1300 and ~1469 cm^{-1} were assigned to C–N stretching vibrations. The peak at ~1145 cm^{-1} is related to C–H deformation vibrations.[48] The peaks at around ~900 and ~1177 cm^{-1} correspond to C–C plane bending in pyrrole and C–N vibrations, respectively.[47,48]

The PANI composite exhibited the characteristic stretching vibrations of quinoid and benzenoid rings at ~1581 and ~1498 cm^{-1}, respectively, confirming the presence of its emeraldine salt. The strong vibration mode at ~1140 cm^{-1} is a measure of

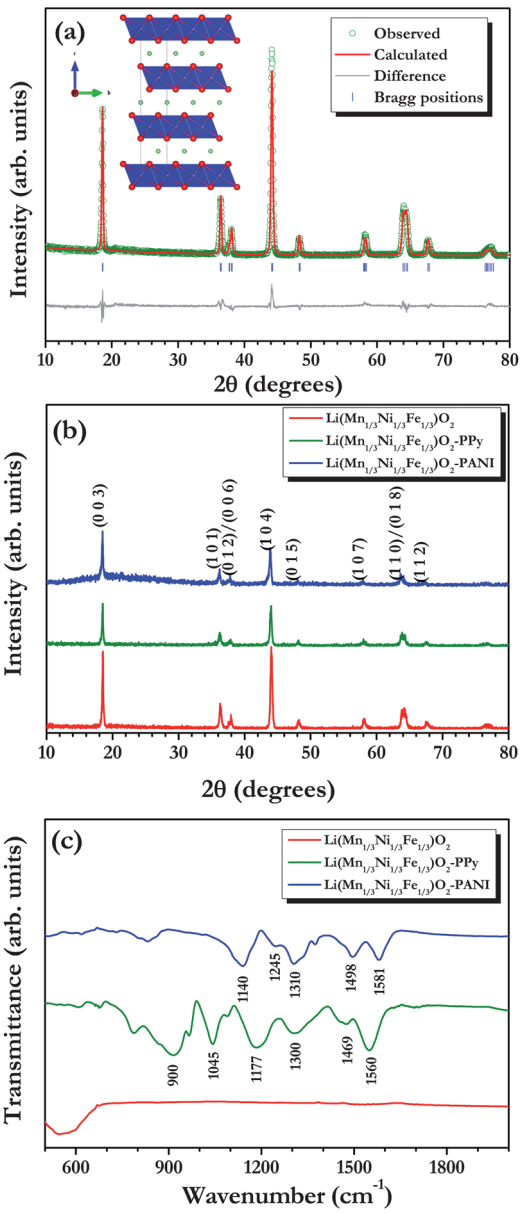

Fig. 2 (a) Rietveld refined X-ray diffraction (XRD) pattern of pristine $Li(Mn_{1/3}Ni_{1/3}Fe_{1/3})O_2$; inset, α-$NaFeO_2$ type crystal structure, (b) XRD patterns of pristine $Li(Mn_{1/3}Ni_{1/3}Fe_{1/3})O_2$, $Li(Mn_{1/3}Ni_{1/3}Fe_{1/3})O_2$–PPy, and $Li(Mn_{1/3}Ni_{1/3}Fe_{1/3})O_2$–PANI composite hybrids and (c) FT-IR spectra of pristine $Li(Mn_{1/3}Ni_{1/3}Fe_{1/3})O_2$, $Li(Mn_{1/3}Ni_{1/3}Fe_{1/3})O_2$–PPy, and $Li(Mn_{1/3}Ni_{1/3}Fe_{1/3})O_2$–PANI composite hybrids.

electrons' delocalization, *i.e.* electronic conductivity.[49] $Li(Mn_{1/3}Ni_{1/3}Fe_{1/3})O_2$–PANI also exhibited bands at ~1310 and ~1245 cm^{-1} attributable to Ph–N and C–NH^+ stretching vibrations, respectively.[50] FT-IR confirmed the existence of polymers (PANI or PPy) in composites with $Li(Mn_{1/3}Ni_{1/3}Fe_{1/3})O_2$.

Samples' morphologies were observed by SEM (Fig. 3). Pristine $Li(Mn_{1/3}Ni_{1/3}Fe_{1/3})O_2$ showed almost evenly shaped particles with sharp edges and uniform size distribution (Fig. 3a). The surfaces of the $Li(Mn_{1/3}Ni_{1/3}Fe_{1/3})O_2$ particles were covered by PPy particles of 100 nm (Fig. 3c). The $Li(Mn_{1/3}Ni_{1/3}Fe_{1/3})O_2$

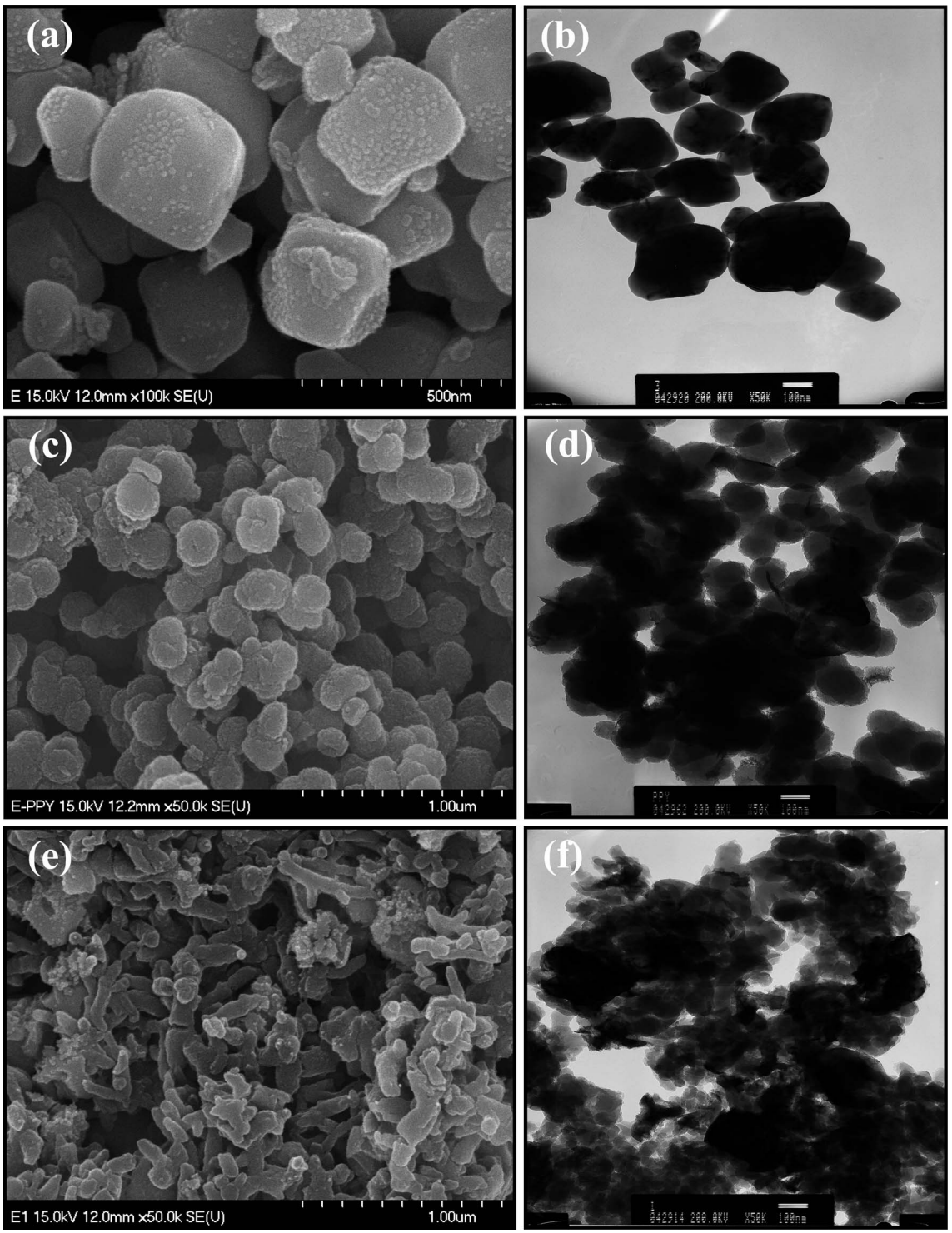

Fig. 3 SEM images of (a) $Li(Mn_{1/3}Ni_{1/3}Fe_{1/3})O_2$ nanoparticles prepared by the mixed hydroxide method, (c) $Li(Mn_{1/3}Ni_{1/3}Fe_{1/3})O_2$–PPy and (e) $Li(Mn_{1/3}Ni_{1/3}Fe_{1/3})O_2$–PANI composite hybrids prepared by chemical polymerization. TEM pictures of the corresponding (b) $Li(Mn_{1/3}Ni_{1/3}Fe_{1/3})O_2$ particles and (d) $Li(Mn_{1/3}Ni_{1/3}Fe_{1/3})O_2$–PPy and (f) $Li(Mn_{1/3}Ni_{1/3}Fe_{1/3})O_2$–PANI composite hybrids.

particles were bound together during the polymerization process, whereas a highly dense, netlike polymer matrix anchored with $Li(Mn_{1/3}Ni_{1/3}Fe_{1/3})O_2$ particles emerged in the PANI composite (Fig. 3d). TEM images of the pristine $Li(Mn_{1/3}Ni_{1/3}Fe_{1/3})O_2$ particles (Fig. 3b) clearly show well-developed particles of 100 to 200 nm with smooth surface morphologies and no aggregation. Clusters of less smooth particles were observed in the composite with PPy (Fig. 3d). However, there was no variation in the sizes of these PPy composite particles during sonication and polymerization. The composite with PANI (Fig. 3e) contained $Li(Mn_{1/3}Ni_{1/3}Fe_{1/3})O_2$ particles within a netlike structure that developed during the chemical polymerization of the aniline monomers. TEM clearly revealed that $Li(Mn_{1/3}Ni_{1/3}Fe_{1/3})O_2$ particles were uniformly covered with PANI fibers. In other words, the active particles are finely connected with the oxide particles during the polymerization process. Such porous nano composites provide voids in the structure which eliminate bulk volume changes during the intercalation and removal of lithium. The flexible structure reduces the mechanical stresses inherent during cycling. This can significantly improve cycling performance at high current rates. In addition, the highly interconnected network of PANI between the $Li(Mn_{1/3}Ni_{1/3}Fe_{1/3})O_2$ particles could enhance the electrode–electrolyte interfacial area by providing a path for better lithium ion diffusion. It could also ensure a high reaction rate, alleviating the intrinsic nature of such Fe-based, layered cathodes. Overall, the PANI-containing composite has a structure conducive to good electrochemical performance.

BET surface areas were calculated to be 5.89, 17.2 and 57.86 $m^2\ g^{-1}$ for $Li(Mn_{1/3}Ni_{1/3}Fe_{1/3})O_2$, $Li(Mn_{1/3}Ni_{1/3}Fe_{1/3})O_2$–PPy and $Li(Mn_{1/3}Ni_{1/3}Fe_{1/3})O_2$–PANI respectively (Fig. S1†). The composite with PANI showed the highest specific surface area due to the presence of clusters or fiber-like polymers. Active materials with high surface area are beneficial for improving Li-ion flux across the electrode–electrolyte interface and can provide facile Li-ion diffusion at high current rates. Therefore, improved electrochemical performance could be expected from the $Li(Mn_{1/3}Ni_{1/3}Fe_{1/3})O_2$–PANI hybrid composite.

Cyclic voltammetry (CV) was used to evaluate the stability and capacitive properties of the electrodes over the applied potential range 0–3 V at different scan rates (Fig. 4a). AC anodes were used with the layered materials used as cathodes in the presence of 1 M $LiPF_6$ EC/DMC (1/1 vol.) electrolyte in two-electrode asymmetric configurations. The active mass loading of pristine $Li(Mn_{1/3}Ni_{1/3}Fe_{1/3})O_2$ and its composite electrode is kept the same for all the electrochemical measurements. At 5 mV s^{-1} (Fig. 4a), the three cells showed more or less rectangular plots with respect to the zero-current line within the measured potential window, suggesting good charge propagation within the electrodes. The CV curves of the cell containing the $Li(Mn_{1/3}Ni_{1/3}Fe_{1/3})O_2$–PANI electrode showed enhanced cathodic and anodic current responses on voltage reversal, indicating higher electrochemical reversibility of the Li-HSC than shown by the other systems (Fig. S2†). The improvement of performance was mainly due to the small $Li(Mn_{1/3}Ni_{1/3}Fe_{1/3})O_2$ particles and the evenly decorated polymer chains, which provided improved conductivity to increase current response. The highly exposed specific surface area and good contact between the current collectors also likely aided performance. Specific capacitance was shown to decrease as the scan rate increased (Fig. 4b). Increasing the scan rate provides less participation of the active material or only the surface of the active material involved in the electrochemical reaction. As a result, Li-HSC delivered less specific capacitance.[19,21,32,45,51] The Li-HSC containing the $Li(Mn_{1/3}Ni_{1/3}Fe_{1/3})O_2$–PANI electrode delivered a specific capacitance of 122 F g^{-1} at a scan rate of 2 mV s^{-1}, greater than 58 and 24 F g^{-1} delivered by the cells containing the $Li(Mn_{1/3}Ni_{1/3}Fe_{1/3})O_2$–PPy composite and pristine $Li(Mn_{1/3}Ni_{1/3}Fe_{1/3})O_2$ electrodes, respectively. The Li-HSC containing PANI composite electrode delivered a very high specific capacitance of ~90 F g^{-1} at a scan rate of 15 mV s^{-1} due to the presence of the highly conducting emeraldine salt of PANI. The open conducting channels and small contributions from polymers' pseudocapacitance properties cannot be avoided in the $Li(Mn_{1/3}Ni_{1/3}Fe_{1/3})O_2$–PANI hybrid.

The Li-HSCs' electrochemical reversibility and durability were assessed by galvanostatic charge–discharge testing at different current densities at ambient temperature (Fig. 5). Typical charge–discharge curves of the three Li-HSCs measured at 0.72 A g^{-1} between 0 and 3 V (Fig. 5a and S3†) show that all the Li-HSCs had linear voltage variation with time (Fig. S3†), suggesting typical capacitance behavior. They do not show well-shaped triangles as symmetric AC/AC systems do because of the different mechanisms involved in charge storage.[16,17,19,21] The Li-HSCs' charge–discharge curves consist of three parts: a resistance part (IR drop), representing voltage changes due to internal resistance; a capacitance component, related to the charge separation between the electrode and electrolyte interface; and a longer time region, the faradaic component, due to the charge transfer reaction of the battery-type Li-insertion material. This reveals that charge storage in the Li-HSCs was by

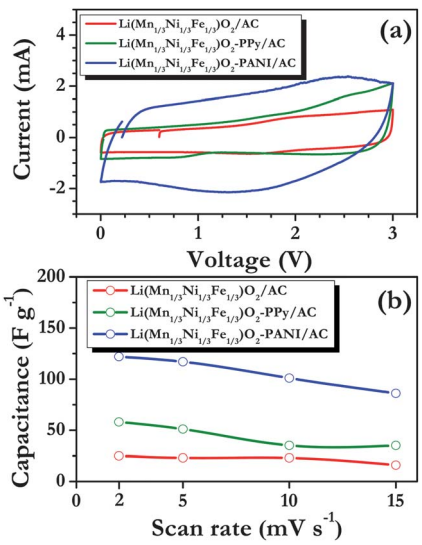

Fig. 4 (a) Cyclic voltammetric traces of Li-ion hybrid supercapacitor $Li(Mn_{1/3}Ni_{1/3}Fe_{1/3})O_2$/AC, $Li(Mn_{1/3}Ni_{1/3}Fe_{1/3})O_2$–PPy/AC, and $Li(Mn_{1/3}Ni_{1/3}Fe_{1/3})O_2$–PANI/AC cells recorded between 0 and 3 V at 5 mV s^{-1} in 1 M $LiPF_6$-EC/DMC (1 : 1 vol.) electrolyte. (b) Plot of specific discharge capacitance *vs.* scan rate.

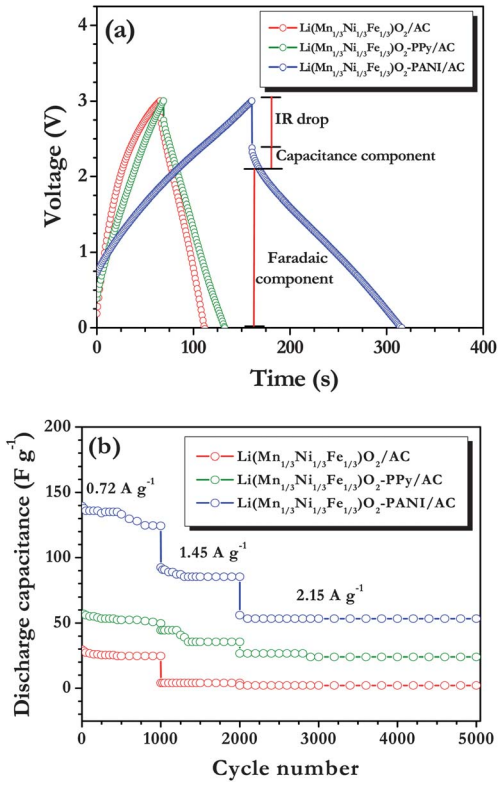

Fig. 5 (a) Typical galvanostatic first charge–discharge curves of $Li(Mn_{1/3}Ni_{1/3}Fe_{1/3})O_2$/AC, $Li(Mn_{1/3}Ni_{1/3}Fe_{1/3})O_2$–PPy/AC, and $Li(Mn_{1/3}Ni_{1/3}Fe_{1/3})O_2$–PANI/AC cells measured at 0.72 A g^{-1} between 0 and 3 V and (b) the cells' cycling profiles.

a combination of both capacitor and battery mechanisms. Discharge capacitances of 29, 57 and 140 F g^{-1} were observed at 0.72 A g^{-1} current density for the Li-HSCs without polymer, with PPy and with PANI composite electrodes, respectively. The different electrochemical behaviors arose due to variations in the morphologies of the electrodes and their inherent conductivity. The observed capacitance of 140 F g^{-1} shown by the Li-HSC with the $Li(Mn_{1/3}Ni_{1/3}Fe_{1/3})O_2$–PANI electrode is the highest reported value for Li-HSCs.[6] The excellent electrochemical behavior shown by this hybrid composite was attributed to the high-surface area, small PANI matrix, which was able to trap more electrolyte solution during charging and discharging. This stabilized the electrode–electrolyte interface, allowing facile redox reactions and improving the capacitive properties during prolonged cycling.

Strong rate performance is required of any electrochemical cell to be used at high power and energy. The Li-HSCs' cycling behaviors were measured at current densities of 0.72–2.15 A g^{-1} (Fig. 5b). The cell with the $Li(Mn_{1/3}Ni_{1/3}Fe_{1/3})O_2$–PANI electrode showed excellent supercapacitive properties; the specific discharge capacitance of ~140 after the first cycle dropped to 125 F g^{-1} after 1000 cycles at 0.72 A g^{-1}, representing a capacitance retention of >90%. The Li-HSCs with $Li(Mn_{1/3}Ni_{1/3}Fe_{1/3})O_2$–PPy and $Li(Mn_{1/3}Ni_{1/3}Fe_{1/3})O_2$ electrodes displayed lower initial specific discharge capacitances, 57 and 29 F g^{-1}, respectively, and retained 87% and 83% capacitance after 1000

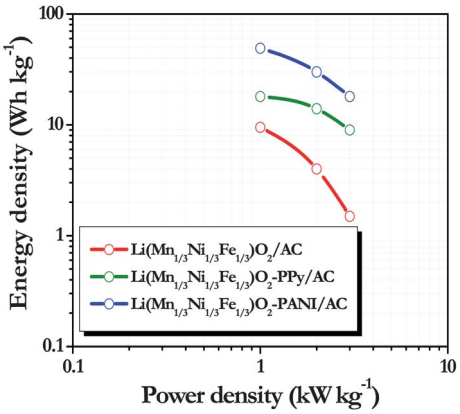

Fig. 6 Ragone plots of the Li-ion hybrid supercapacitors calculated from the galvanostatic cycling profiles (Fig. 5).

cycles under similar conditions. The Li-HSCs were further subjected to high current rates over the same potential range. The Li-HSC with a pristine electrode performed poorly. Those with polymers showed enhanced electrochemical performance at 2.15 A g^{-1}: the cell with the $Li(Mn_{1/3}Ni_{1/3}Fe_{1/3})O_2$–PPy electrode delivered 27 F g^{-1} and that with $Li(Mn_{1/3}Ni_{1/3}Fe_{1/3})O_2$–PANI has 56 F g^{-1}, both without any appreciable capacitance fade. The high current performance of the cell with the $Li(Mn_{1/3}Ni_{1/3}Fe_{1/3})O_2$–PANI electrode was due to its large specific surface area, which increased the number of active sites for redox reactions. The highly porous network of the PANI structure anchored with $Li(Mn_{1/3}Ni_{1/3}Fe_{1/3})O_2$ particles also enhanced the conductivity by allowing penetration of more electrolyte and protected against the mechanical stresses inherent during high-rate cycling.

The cells' specific energy (S_{ED}) and power (S_{PD}) densities were calculated from the galvanostatic charge–discharge results as follows.

$$S_{PD}\ (\mathrm{W\ kg^{-1}}) = IV/2m \quad (1)$$

$$S_{ED}\ (\mathrm{W\ h\ kg^{-1}}) = S_{PD} \times t/3600 \quad (2)$$

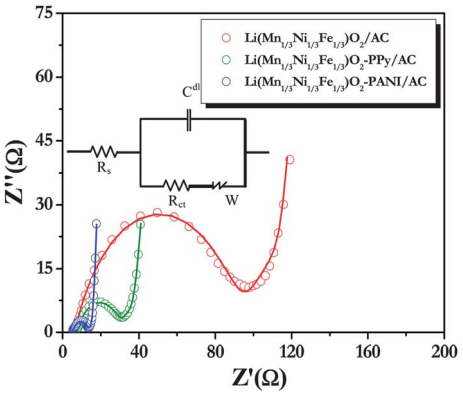

Fig. 7 Electrochemical impedance spectra of $Li(Mn_{1/3}Ni_{1/3}Fe_{1/3})O_2$/AC, $Li(Mn_{1/3}Ni_{1/3}Fe_{1/3})O_2$–PPy/AC, and $Li(Mn_{1/3}Ni_{1/3}Fe_{1/3})O_2$–PANI/AC cells measured after 5000 cycles. Symbols and lines correspond to experimental and fitted data, respectively. Inset: equivalent circuit.

where I is the applied current, V is the cell voltage, t is the discharge time and m is the total mass of the active materials in both electrodes.[16–19] The Ragone plots (Fig. 6) show that the cell with the $Li(Mn_{1/3}Ni_{1/3}Fe_{1/3})O_2$–PANI electrode delivered very high S_{ED} and S_{PD} even under harsh cycling. Its maximum energy density was ~49 W h kg^{-1}, much greater than ~18 and 10 W h kg^{-1} respectively shown by the cells with $Li(Mn_{1/3}Ni_{1/3}Fe_{1/3})O_2$–PPy and $Li(Mn_{1/3}Ni_{1/3}Fe_{1/3})O_2$ electrodes, respectively. The cell with a PANI composite electrode delivered S_{ED} and S_{PD} values that are among the best reported for Li-HSCs (Table S1†) with Li-intercalating materials in non-aqueous medium, for instance $LiCoO_2$/AC:$Li_4Ti_5O_{12}$ (energy density: ~25 W h kg^{-1}),[2] AC/$LiCrTiO_4$ (energy density of ~25 W h kg^{-1}),[16] CNT/TiO_2-B (energy density: ~13 W h kg^{-1}),[21] CNT/V_2O_5 (energy density: ~18 W h kg^{-1}),[19] AC/TiP_2O_7 (energy density: ~13 W h kg^{-1})[18] and AC/$LiTi_2(PO_4)_3$ (energy density: ~14 W h kg^{-1}).[17]

EIS validated the effects of the polymers on the electrical conductivity of the $Li(Mn_{1/3}Ni_{1/3}Fe_{1/3})O_2$ particles. Typical Nyquist plots of the cells (Fig. 7) were recorded after 5000 galvanostatic cycles at various current densities. The EIS traces were fitted according to an equivalent circuit (inset, Fig. 6). They each show two regions: a semi-circle at high frequency, assigned to charge transfer resistance (R_{ct}), and linear portion at low frequency, the Warburg tail due to diffusion-controlled processes. The cell with the PANI composite electrode showed an R_{ct} of 9 Ω, much lower than 101 and 28 Ω, respectively, shown by the cells with $Li(Mn_{1/3}Ni_{1/3}Fe_{1/3})O_2$–PPy and $Li(Mn_{1/3}Ni_{1/3}Fe_{1/3})O_2$ electrodes. This demonstrates that PANI significantly increased the electronic conductivity of the electrode and thus improved cycling performance, which led to the increase in supercapacitive performance and energy storage capability.

Conclusion

A new class of high-performance, hybrid supercapacitor (Li-HSC) was constructed with novel organic–inorganic hybrid composites of a conducting polymer with a Li-intercalating component. The Li-HSC fabricated with a $Li(Mn_{1/3}Ni_{1/3}Fe_{1/3})O_2$–PANI cathode and AC anode exhibited very strong supercapacitive properties, delivering a maximum specific capacitance of ~140 F g^{-1} and an energy density of 49 W h kg^{-1}. It overcame the disadvantage of electrolyte depletion during cycling due to its structure containing a porous polymer network. This led to increased energy density at high current rates. Such devices are potentially useful in low-environmental impact devices such as hybrid and electric vehicles that require high specific energy, high power, improved rate performance, good cycle life, high safety and low cost. Supercapacitors containing composites of Li-insertion materials and conducting polymers in non-aqueous media represent a new class of improved high-energy density electrochemical storage devices.

Acknowledgements

This work was supported by the IT R&D program of MKE/KEIT. [KI002176, Development of 3.6 Ah Class Cylindrical Type Lithium Secondary Battery.]

References

1 G. G. Amatucci, F. Badway, A. Du Pasquier and T. Zheng, *J. Electrochem. Soc.*, 2001, **148**, A930.
2 I. Plitz, A. DuPasquier, F. Badway, J. Gural, N. Pereira, A. Gmitter and G. G. Amatucci, *Appl. Phys. A: Mater. Sci. Process.*, 2006, **82**, 615.
3 O. K. Park, Y. Cho, S. Lee, H.-C. Yoo, H.-K. Song and J. Cho, *Energy Environ. Sci.*, 2011, **4**, 1621.
4 D. Cericola and R. Kötz, *Electrochim. Acta*, 2012, **72**, 1.
5 R. Kötz and M. Carlen, *Electrochim. Acta*, 2000, **45**, 2483.
6 K. Naoi and P. Simon, *Electrochem. Soc. Interface*, 2008, **17**, 34.
7 P. Simon and Y. Gogotsi, *Nat. Mater.*, 2008, **7**, 845.
8 V. V. N. Obreja, *Phys. E*, 2008, **40**, 2596.
9 M. Inagaki, H. Konno and O. Tanaike, *J. Power Sources*, 2010, **195**, 7880.
10 L. Wei and G. Yushin, *Nano Energy*, 2012, **1**, 552.
11 T. C. Liu, W. G. Pell and B. E. Conway, *Electrochim. Acta*, 1999, **44**, 2829.
12 Z. Fan, J. Yan, T. Wei, L. Zhi, G. Ning, T. Li and F. Wei, *Adv. Funct. Mater.*, 2011, **21**, 2366.
13 N. W. Duffy, W. Baldsing and A. G. Pandolfo, *Electrochim. Acta*, 2008, **54**, 535.
14 T. Brousse, R. Marchand, P.-L. Taberna and P. Simon, *J. Power Sources*, 2006, **158**, 571.
15 W. Deng, X. Ji, Q. Chen and C. E. Banks, *RSC Adv.*, 2011, **1**, 1171.
16 V. Aravindan, W. Chuiling and S. Madhavi, *J. Mater. Chem.*, 2012, **22**, 16026.
17 V. Aravindan, W. Chuiling, M. V. Reddy, G. V. S. Rao, B. V. R. Chowdari and S. Madhavi, *Phys. Chem. Chem. Phys.*, 2012, **14**, 5808.
18 V. Aravindan, M. V. Reddy, S. Madhavi, S. G. Mhaisalkar, G. V. Subba Rao and B. V. R. Chowdari, *J. Power Sources*, 2011, **196**, 8850.
19 V. Aravindan, Y. L. Cheah, W. F. Mak, G. Wee, B. V. R. Chowdari and S. Madhavi, *ChemPlusChem*, 2012, **77**, 570.
20 R. Vasanthi, D. Kalpana and N. G. Renganathan, *J. Solid State Electrochem.*, 2008, **12**, 961.
21 Q. Wang, Z. H. Wen and J. H. Li, *Adv. Funct. Mater.*, 2006, **16**, 2141.
22 L.-M. Chen, Q.-Y. Lai, Y.-J. Hao, Y. Zhao and X.-Y. Ji, *J. Alloys Compd.*, 2009, **467**, 465.
23 Y.-G. Wang and Y.-Y. Xia, *Electrochem. Commun.*, 2005, **7**, 1138.
24 A. Du Pasquier, A. Laforgue and P. Simon, *J. Power Sources*, 2004, **125**, 95.
25 X.-L. Wu, L.-Y. Jiang, F.-F. Cao, Y.-G. Guo and L.-J. Wan, *Adv. Mater.*, 2009, **21**, 2710.
26 S.-B. Ma, K.-W. Nam, W.-S. Yoon, X.-Q. Yang, K.-Y. Ahn, K.-H. Oh and K.-B. Kim, *Electrochem. Commun.*, 2007, **9**, 2807.
27 X. Hu, Z. Deng, J. Suo and Z. Pan, *J. Power Sources*, 2009, **187**, 635.

28 C. Xu, F. Kang, B. Li and H. Du, *J. Mater. Res.*, 2012, **25**, 1421.
29 H. Wu, C. V. Rao and B. Rambabu, *Mater. Chem. Phys.*, 2009, **116**, 532.
30 Y. Xue, Y. Chen and M.-L. Zhang, *Mater. Chem. Phys.*, 2008, **110**, 486.
31 K. Karthikeyan, V. Aravindan, S. B. Lee, I. C. Jang, H. H. Lim, G. J. Park, M. Yoshio and Y. S. Lee, *J. Alloys Compd.*, 2010, **504**, 224.
32 K. Karthikeyan, V. Aravindan, S. B. Lee, I. C. Jang, H. H. Lim, G. J. Park, M. Yoshio and Y. S. Lee, *J. Power Sources*, 2010, **195**, 3761.
33 N. Yabuuchi and T. Ohzuku, *J. Power Sources*, 2003, **119–121**, 171.
34 S. Okada and J.-I. Yamaki, *J. Ind. Eng. Chem.*, 2004, **10**, 1104.
35 X. Xia, Q. Hao, W. Lei, W. Wang, H. Wang and X. Wang, *J. Mater. Chem.*, 2012, **22**, 8314.
36 Jaidev, R. I. Jafri, A. K. Mishra and S. Ramaprabhu, *J. Mater. Chem.*, 2011, **21**, 17601.
37 L. Zheng, Y. Xu, D. Jin and Y. Xie, *Chem.–Asian J.*, 2011, **6**, 1505.
38 Z.-A. Hu, Y.-L. Xie, Y.-X. Wang, L.-P. Mo, Y.-Y. Yang and Z.-Y. Zhang, *Mater. Chem. Phys.*, 2009, **114**, 990.
39 Z. H. Dong, Y. L. Wei, W. Shi and G. A. Zhang, *Mater. Chem. Phys.*, 2011, **131**, 529.
40 K. S. Park, S. B. Schougaard and J. B. Goodenough, *Adv. Mater.*, 2007, **19**, 848.
41 Y.-H. Huang and J. B. Goodenough, *Chem. Mater.*, 2008, **20**, 7237.
42 W.-M. Chen, Y.-H. Huang and L.-X. Yuan, *J. Electroanal. Chem.*, 2011, **660**, 108.
43 E. Perez-Cappe, Y. Mosqueda, R. Martinez, C. R. Milian, O. Sanchez, J. A. Varela, A. Hortencia, E. Souza, P. Aranda and E. Ruiz-Hitzky, *J. Mater. Chem.*, 2008, **18**, 3965.
44 P. Zhang, L. Zhang, X. Ren, Q. Yuan, J. Liu and Q. Zhang, *Synth. Met.*, 2011, **161**, 1092.
45 K. Karthikeyan, V. Aravindan, S. B. Lee, I. C. Jang, H. H. Lim, G. J. Park, M. Yoshio and Y. S. Lee, *J. Alloys Compd.*, 2010, **504**, 224.
46 C. Q. Feng, S. Y. Chew, Z. P. Guo, J. Z. Wang and H. K. Liu, *J. Power Sources*, 2007, **174**, 1095.
47 X. Yang and L. Li, *Synth. Met.*, 2010, **160**, 1365.
48 S. Tamil Selvan, *Chem. Commun.*, 1998, 351.
49 M. Baibarac, I. Baltog, S. Lefrant, J. Y. Mevellec and O. Chauvet, *Chem. Mater.*, 2003, **15**, 4149.
50 Y. Furukawa, F. Ueda, Y. Hyodo, I. Harada, T. Nakajima and T. Kawagoe, *Macromolecules*, 1988, **21**, 1297.
51 K. Zaghib, J. B. Goodenough, A. Mauger and C. Julien, *J. Power Sources*, 2009, **194**, 1021.

